water

MDPI

Article

Local Water Inrush Risk Assessment Method Based on Moving Window and Its Application in the Liangshuijing Mining Area

Chengyue Gao [1], Dangliang Wang [1,*], Jin Ma [1], Kerui Liu [1] and Yafei Fang [2]

[1] School of Resources and Geosciences, China University of Mining and Technology, Xuzhou 221116, China; chengyueg@cumt.edu.cn (C.G.); kerui.liu@cumt.edu.cn (K.L.)
[2] Shaanxi Energy Liangshuijing Mining Co., Ltd., Yulin 719315, China; yafeifang147@outlook.com
* Correspondence: wangdangliang@cumt.edu.cn

Abstract: Most of the existing coal mine water inrush risk assessment methods are global assessment methods, which have the following problems: they ignore the difference in importance of the evaluation indicators at different locations in the study area and assign the same weight value; the area of the danger zone in the evaluation results is thus too large. The evaluation results improve the prediction accuracy by reducing the safe zone area. To address the aforementioned issues, this study employs a local analysis method based on a moving circular window, taking into account the spatial heterogeneity of criterion indicators in the decision-making process. By traversing each position of the raster with a circular moving window, the method performs local standardization and calculates local weights of indicators within the local window range. Based on the obtained maps of locally standardized evaluation criteria and local weights, a local water inrush risk assessment model is established using Geographic Information Systems (ArcGIS), considering the differences in the importance of evaluation indicators within the study area. Taking the Liangshuijing mining area as an example, both global and local evaluation models were employed to assess its water inrush risk. The evaluation results obtained from these two models were compared and validated against geological survey data and historical water inrush points. The comparative analysis between the two methods reveals that the local evaluation model demonstrates higher accuracy. It offers a more precise delineation of the distribution of water inrush risk zones, which better corresponds to the actual conditions within the mine. The localized water inrush risk assessment method proposed in this paper breaks away from the traditional approach of uniformly weighting evaluation indicators across the entire area, offering a novel method for assessing water inrush risk.

Keywords: roof water inrush; MAHP; local water inrush risk assessment method

Citation: Gao, C.; Wang, D.; Ma, J.; Liu, K.; Fang, Y. Local Water Inrush Risk Assessment Method Based on Moving Window and Its Application in the Liangshuijing Mining Area. *Water* **2024**, *16*, 1083. https://doi.org/10.3390/w16081083

Academic Editor: Maurizio Barbieri

Received: 11 March 2024
Revised: 31 March 2024
Accepted: 3 April 2024
Published: 10 April 2024

1. Introduction

Due to the depletion of coal reserves in eastern China, China's northwest mining regions have become the primary coal-producing regions [1–3]. The major geological hazard faced by coal mines in the western regions is roof water inrush, which limits safe and efficient coal mining [1–3]. Numerous roof water inrush disasters have occurred in the western mining regions in recent years, causing significant casualties and substantial financial damages [1–3]. The Min Dong coal mine in Inner Mongolia suffered a roof water inrush accident on 27 September 2023, which caused three fatalities and a direct economic loss of CNY 3.7772 million [4]. On 27 January 2023, a roof water inrush accident occurred in Jushan Coal Mine in Shanxi, resulting in fatalities and direct economic losses of CNY 8.7612 million [4]. In 2021, a major water inrush accident occurred at the Fengyuan Coal Mine in Bayangol County, Changji Prefecture, Xinjiang, resulting in 21 fatalities and economic losses of CNY 70.672 million [4]. On 14 August 2021, a water/sand inrush incident unfolded at Chaida'er Coal Mine in Qinghai, leading to 20 fatalities and direct financial losses totaling around CNY 53.91 million [4]. Therefore, conducting accurate evaluations of mine water inrush risk is of significant importance for averting and managing roof water hazards, enabling the early initiation of prevention measures, and guaranteeing the secure mining of coal [5].

Existing studies commonly utilize global evaluation methods to assess the risk of roof and floor water inrush. For instance, methods such as the three-map double prediction method [6–9] and the vulnerability index method [10–13] have been employed. However, these evaluation methods share a common issue in the allocation of weights to evaluation indicators. Specifically, they assign the same weight values to evaluation indicators across all locations within the study area [14–23]. This implies that existing evaluation methods do not account for the varying relative importance of evaluation indicators at different locations within the study area, resulting from differences in the magnitude of attribute values. In other words, the same indicator should be assigned different weight values at different locations within the study area due to variations in the attribute values of the evaluation indicators. In the evaluation of roof water inrush risk, when the water pressure is higher or the thickness of the aquifuge is thinner at a specific unit location within the study area, it indicates that the water pressure or aquifuge thickness has a stronger controlling effect on roof water inrush compared to other units. In this context, water pressure or aquifuge thickness serves as the primary determining factor for roof water inrush at that unit location. Therefore, the weight of the evaluation indicator for water pressure or aquifuge thickness at this unit location should be higher than in other areas to reflect the influence of spatial variations in evaluation attribute values on the control of water inrush. However, in a global evaluation model, since the weights at all locations are the same, regardless of the weighting calculation method used, it is impossible to reflect the differences in weights among different regions. Furthermore, the evaluation results of this unit may be neutralized by other evaluation indicators. The more evaluation indicators are selected, the more evenly distributed the weights are, increasing the likelihood of incorrect judgments. This may result in the final evaluation results deviating from the actual situation, making it difficult to accurately highlight the severity of the problem. Consequently, the evaluation loses its objectivity and fairness. Additionally, the evaluation results from global models suffer from issues such as the clustering of high-risk water inrush areas, large distribution areas of risk zones, lack of specificity in delineating risk zone boundaries, and a reduction in safe zone areas to improve prediction accuracy [14,15,20,23]. The widespread distribution of risk zones implies that coal companies will have to expend significant financial and material resources to carry out water prevention and control efforts. Existing evaluation methods are unable to effectively guide coal mines in water management and control efforts, leading to significant levels of uncertainty and blind spots in these efforts.

To address the aforementioned issues, this study employed a local analysis method based on a moving circular window, considering the spatial heterogeneity of criterion indicators in the decision-making process. By traversing each position of the raster with a circular moving window, the method performed local standardization and calculated local weights of indicators within the local window range. Based on the locally standardized evaluation criteria and local weights, a local water inrush risk assessment model was established using geographic information systems (ArcGIS). Taking the Liangshuijing mining area as an example, both global and local evaluation models were utilized to assess its water inrush risk. A comparative analysis of the evaluation results from these two models revealed that the local evaluation model demonstrated higher accuracy. It provided a more precise delineation of the distribution of water inrush risk zones, which better corresponded to the actual conditions within the mine.

2. Study Area and Data

The study area is situated approximately 16 km west of Shenmu County, in Shaanxi Province. The Liangshuijing coal mine encompasses 68.9 square kilometers and is situated in the northwest inland region. Its climate is typically characterized as temperate semi-arid continental, with an annual precipitation averaging 435.7 mm and an annual evaporation averaging 1774.1 mm. Figure 1 depicts the geographic location of the study area. The mine is authorized for an annual production capacity of 8 million tons, with an operational lifespan projected at 46.8 years. The working face adopts the longwall fully mechanized mining method. The primary coal seam in the study area is the 4^{-2} coal seam, located at the uppermost portion of the second section of the Yan'an Formation within the Jurassic system. The coal seam mining elevation ranges from 1120 to 1080 m, with a depth of burial ranging from 13.45 to 160.92 m.

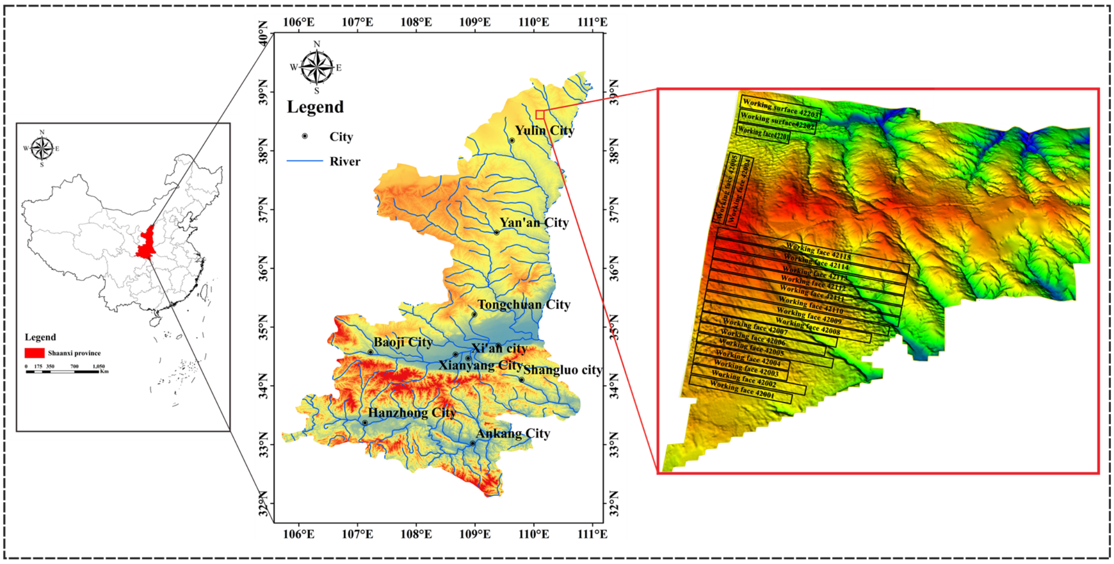

Figure 1. Geographical location map of the Liangshuijing coal mine [22].

The geological structure of the study area is undeveloped, with gentle strata and a dip angle of less than 1°. It is characterized by wide and gentle undulations of synclines, with no major folds, faults, or magmatic activities. The Formations (Fmts) in the study area, from oldest to youngest, are as follows: Yongping Fmt (T_3y), Yan'an Fmt (J_2y), Zhiluo Fmt (J_2z), Xinjiang Fmt (N_2b), Lishi Fmt (Q_2l), Salawusu Fmt ($Q_3{}^s$), and Quaternary Holocene Aeolian Sand ($Q_4{}^{eol}$). Figure 2 presents the hydrogeological cross-section of the study area [18–22].

For assessing roof water inrush risk in coal mines, seven evaluation indicators were selected [17,21]: water abundance of aquifer (WWA), aquifer permeability (AP), aquifer thickness (At), aquifuge thickness (AFT), coal seam thickness (CT), mining depth (MD), overburden failure height (OFH). The rationale behind the selection of each evaluation indicator is outlined below.

WWA: The WWA refers to its ability to discharge water. During coal seam mining, connecting water-bearing fractured zones to the aquifer can lead to increased water inflow into the working face. The WWA directly influences the amount of water released, thus heightening the risk of water inrush. The unit water inflow rate (q) from pumping tests conducted in boreholes was employed to quantify the WWA. The entire study area's zoning map of WWA was obtained using ArcGIS (Esri Inc., Redlands, CA, USA, version 10.8) Kriging interpolation (Figure 3a).

AT: The AT determines the size of the water storage space within the formation. As the AT increases, so does the capacity for water storage, resulting in a larger volume of stored water. Consequently, the risk of roof water inrush escalates during coal seam mining. In this study, the thickness data of aquifers at borehole locations in the study area were collected, and the study area zoning map of AT was generated using the ArcGIS Kriging interpolation method (Figure 3b).

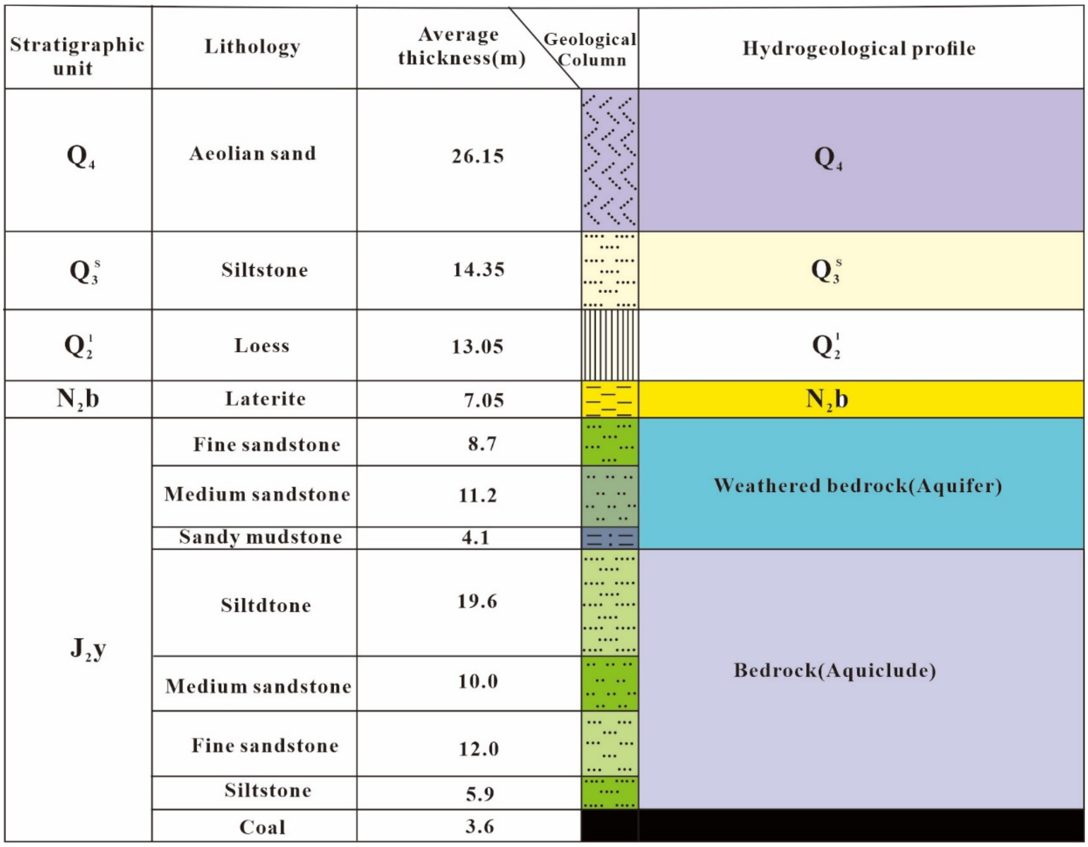

Figure 2. Hydrogeological cross-sectional diagram of the study area [18,22].

AP: The AP reflects its hydraulic conductivity; the higher the AP, the greater its ability to transmit water, resulting in a higher risk of water inrush from the roof strata. In this study, the permeability of the aquifer was quantified using measured permeability coefficients obtained from pumping tests conducted in boreholes within the study area. The zoning map of AP was generated using the ArcGIS Kriging interpolation method (Figure 3c).

AFT: The aquifuge functions to impede the flow of water between the aquifer and the coal seam, thereby reducing the height of fracture development caused by mining activity. As the thickness of the aquifuge increases, the likelihood of fractures connecting to the aquifer decreases, leading to a decreased risk of water inrush from the roof strata in coal mining operations. Utilizing statistical data of AFT obtained from borehole locations within the research region, the zoning map of AFT was generated using the ArcGIS Kriging interpolation method (Figure 3d).

CT: As the thickness of the coal seam increases during mining operations, it induces greater disruption to the overlying strata, consequently causing more pronounced deformation and damage to the roof strata. As a result, the likelihood of roof water inrush escalates with the CT increase. Based on statistical data obtained from exploration boreholes within the study area, the zoning map of 4^{-2} coal-seam thickness was generated using the ArcGIS Kriging interpolation method (Figure 3e).

MD: The MD has a significant impact on the stress changes and overlying strata failure height after coal mining. Deeper coal seams result in a higher original stress of the overlying strata, which in turn leads to an increased failure height of the overlying strata and a heightened susceptibility to water inrush accidents during coal mining. This study utilized the depth data of the 4-2 coal seams obtained from exploration boreholes within the study area to create zoning maps of 4-2 coal depth using the ArcGIS Kriging interpolation method (Figure 3f).

OFH: Coal mining results in the movement, deformation, and fracturing of the overlying strata, leading to the formation of fracture zones and collapse zones within the overlying strata. When these fracture zones connect with the aquifer, they form pathways for water inrush into the mine. As the water-conducting fracture zones become more developed, the risk of water inrush from the overlying strata increases. Liangshuijing Coal Mine conducted on-site measurements of OFH and established a relationship between coal thickness and overlying failure height according to Equation (1).

$$h = 19.51 \cdot m \quad (1)$$

where m is the coal seam thickness, and h is the overburden failure height.

The OFH at each borehole location was calculated using Equation (1). Then, the zoning map of OFH for the 4^{-2} coal seam was generated using the Kriging interpolation tool in ArcGIS (Figure 3g).

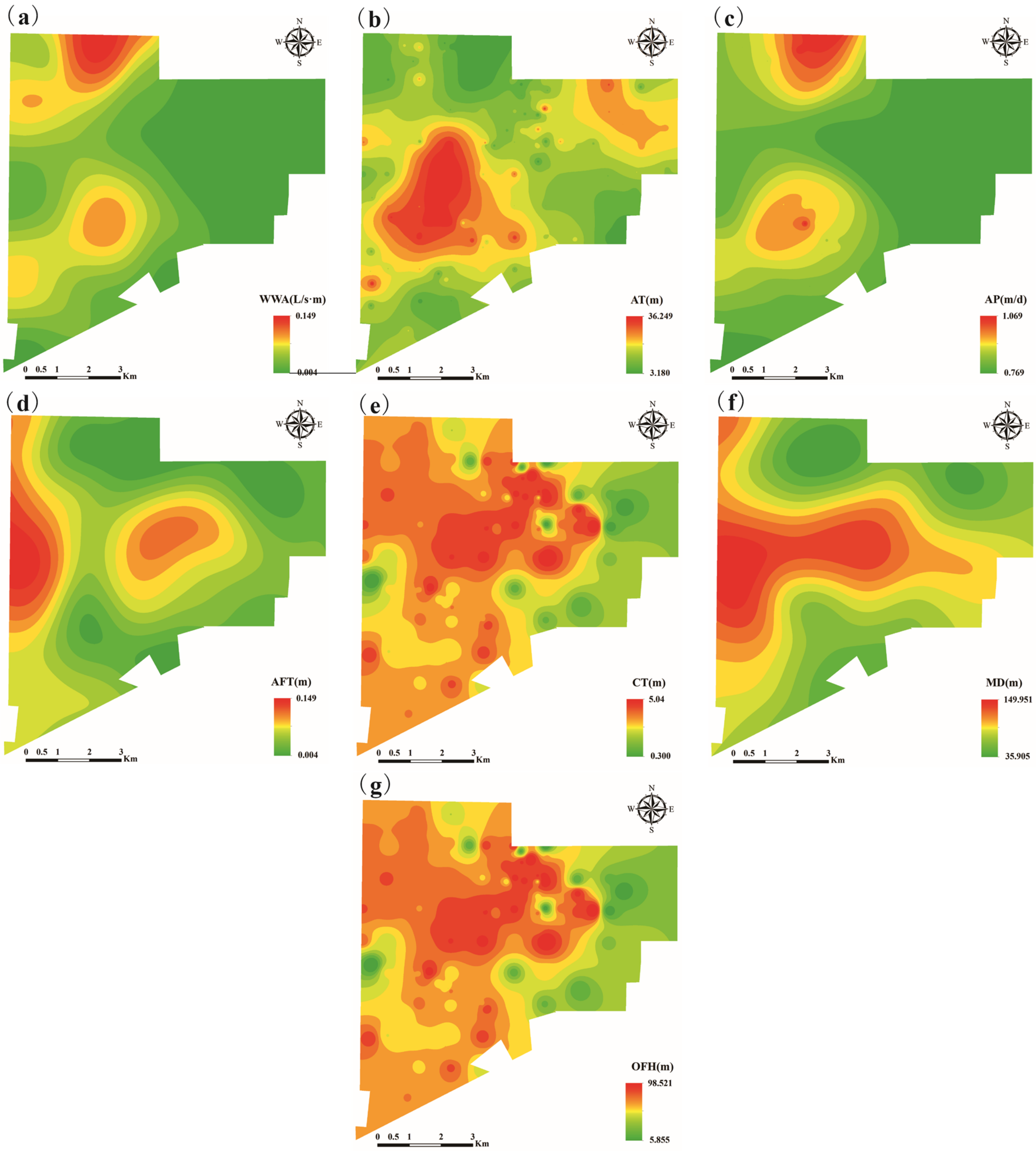

Figure 3. Thematic map of evaluation indicator attribute values obtained using ordinary Kriging interpolation: (**a**) WWA; (**b**) AT; (**c**) AP; (**d**) AFT; (**e**) CT; (**f**) MD; and (**g**) OFH.

3. Methodology

3.1. MAHP

The Analytic Hierarchy Process (AHP) is a commonly employed method for calculating the weights of evaluation indicators in water inrush risk assessment. However, it encounters the following issues:

(1) AHP suffers from a problem of excessive subjectivity during the calculation of evaluation indicators' weights, relying too heavily on subjective scoring judgments by experts [24,25].
(2) The relative importance between evaluation indicators typically requires precise numerical descriptions, which experts often struggle to provide accurately.
(3) In cases where the relative significance of evaluation indicators is similar, it becomes challenging to ascertain which indicator holds greater importance.

To overcome these shortcomings, this study adopts the Monte Carlo Analytic Hierarchy Process (MAHP) method to calculate the weights of evaluation indicators. This method addresses the aforementioned issues by introducing a probability distribution of expert scores. The Monte Carlo AHP calculation process is illustrated in Figure 4, and specific calculation steps can be found in previous publications by the authors [23,26–28].

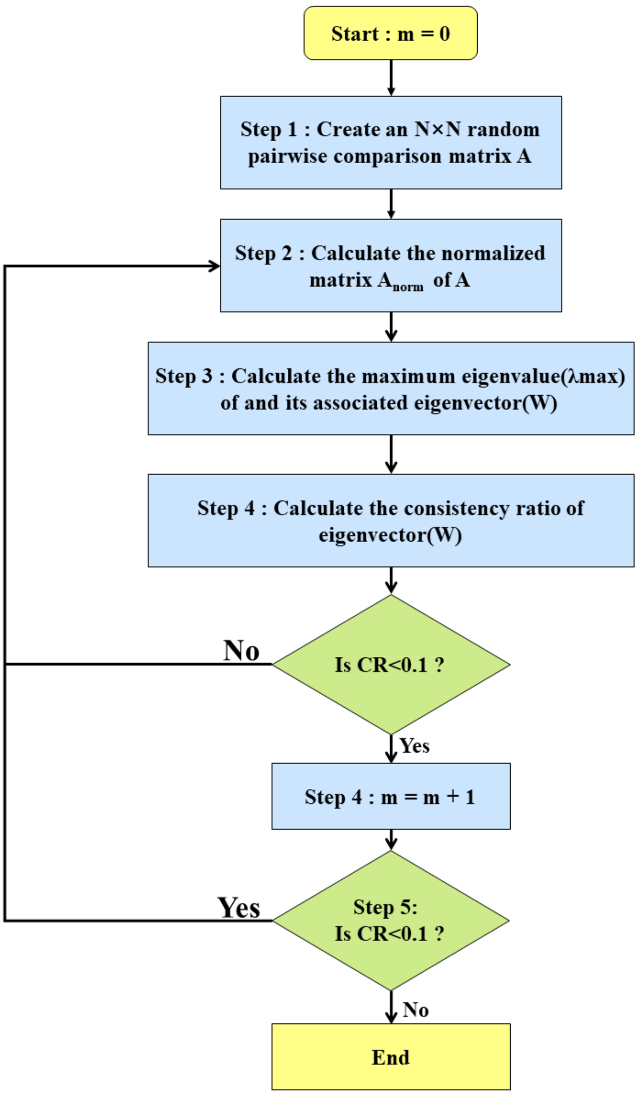

Figure 4. Monte Carlo analytical hierarchy process flow chart [22].

3.2. Global Evaluation Method

The majority of prevailing methods for assessing water inrush risk are global assessment approaches, and their specific computation procedures are outlined as follows:

(1) Global standardization of evaluation indicator attribute data.

The evaluation criterion attribute data are standardized using Equations (2) and (3). Equation (2) is employed for standardization if the contribution of the evaluation criterion to water inrush is positively correlated. Conversely, if it is negatively correlated, Equation (3) is used for standardization.

$$\overline{a_{ij}} = \frac{a_{ij} - \min\{a_{ij}\}}{r_j} \tag{2}$$

$$\overline{a_{ij}} = \frac{\max\{a_{ij}\} - a_{ij}}{r_j} \tag{3}$$

(2) Establishment of a global evaluation model.

On the basis of standardizing the thematic map of evaluation indicators, combined with the evaluation indicators' weights calculated using the MAHP method, the global evaluation model for water inrush risk is established using Equation (4):

$$RI(GA) = \sum_{i=1}^{n} w_i \cdot f(x, y) \tag{4}$$

where RI (GA) is the global water inrush risk coefficient, w_{i} is the weight of evaluation indicators, n is the number of evaluation indicators, and $f(x,y)$ is the dimensionless attribute map of evaluation indicators.

3.3. Local Evaluation Method

In order to reflect the differences at different locations within the study area, this paper adopts a local water inrush risk assessment method, the calculation process of which is as follows:

(1) Local standardization of evaluation indicators.

This study adopts the circular moving window method for the local standardization of evaluation indicator maps, as illustrated in Figure 5. Circular windows are commonly used to determine the raster objects contained within a local range, with a specific raster cell as the focus. By creating a circular window and traversing each position of the raster grid using a moving window approach, all raster cells within the window range are considered as local analysis objects. Local statistical analysis of raster cell attribute values or local operations using functions are then applied to achieve the local standardization of evaluation indicator layers. If the contribution of the evaluation indicator to the risk of roof water inrush is positively correlated, Equation (5) is used for standardizing the indicator map within the circular window; conversely, Equation (6) is applied for standardization if the correlation is negative [28–31].

$$f(x_{ij}) = \frac{x_{ij} - \min\limits_{Q}\{x_{ij}\}}{r_j} \tag{5}$$

$$f(x_{ij}) = \frac{\max\limits_{Q}\{x_{ij}\} - x_{ij}}{r_j} \tag{6}$$

where x_{ij} is the attribute value at the focal point, $\min\limits_{Q}\{x_{ij}\}$ and $\max\limits_{Q}\{x_{ij}\}$ are the local minimum and maximum values within the window, and r_j is the range of attribute values within the circular window. $r_j = \max\limits_{Q}(x_{ij}) - \min\limits_{Q}(x_{ij})$.

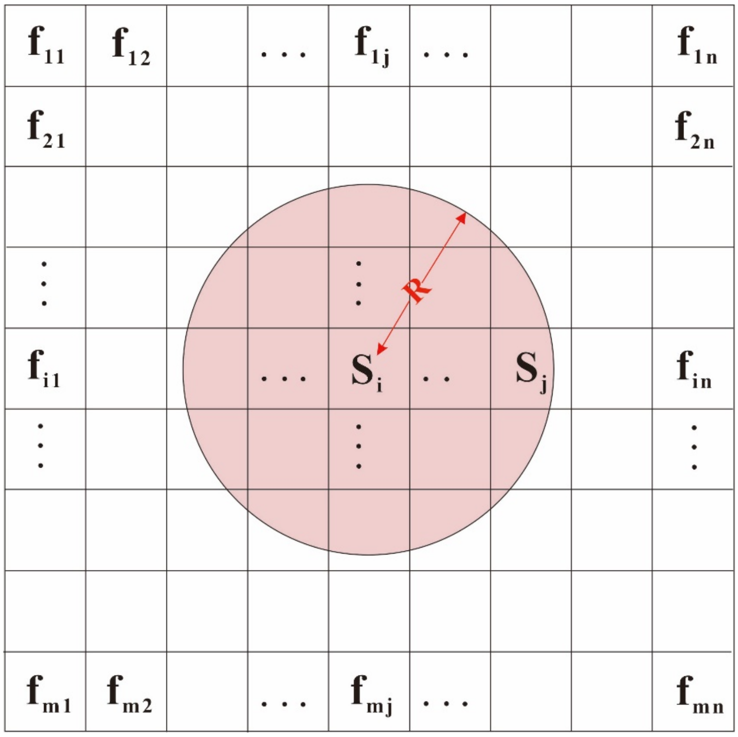

Figure 5. Localized standardization circular moving window.

(2) Localized weighting of evaluation indicators.

The relative importance of evaluation indicators varies with geographical location. After specifying the size of the local area, the local weights of evaluation indicators are calculated using Equation (7).

$$w_j^q = \frac{\frac{w_j r_j^q}{r_j}}{\sum\limits_{i=1}^{n} \frac{w_j r_j^q}{r_j}},\ 0 \le w_j^q \le 1,\ \sum_{j=1}^{n} w_j^q = 1, \sum_{i=1}^{n} w_j^q = 1, \tag{7}$$

where $w_j{}^q$ is the local weight of the evaluation indicator; w_j is the global weight of the evaluation criterion obtained using the MAHP calculation results in Section 3.1; r_j is the global criterion attribute value range; and $r_j{}^q$ is the local attribute value range.

(3) Establishing the local water inrush risk assessment model.

Building upon the thematic maps of evaluation indicators after local standardization and the thematic maps of local weights of evaluation indicators, a local water inrush risk assessment model is established, as shown in Equation (8).

$$RI(LC) = \sum_{i=1}^{n} w(x,y) \cdot f(x,y) \tag{8}$$

where $w(x,y)$ is the thematic map of localized weights for evaluation factors, and $f(x,y)$ is the dimensionless attribute map after the localized standardization of evaluation indicators.

4. Results

4.1. Standardization of Evaluation Indicators

4.1.1. Global Standardization of Evaluation Indicators

The evaluation indicators are standardized globally using Equations (2) and (3). Among these, six factors including WWA, AP, AT, CT, MD, and OFH, which are positively correlated with the top plate water inrush risk, are standardized using Equation (3).

On the other hand, the aquifuge thickness, which is negatively correlated with the top plate water inrush risk, is standardized using Equation (4). Non-dimensional maps for each evaluation indicator are obtained in ArcGIS (Figure 6).

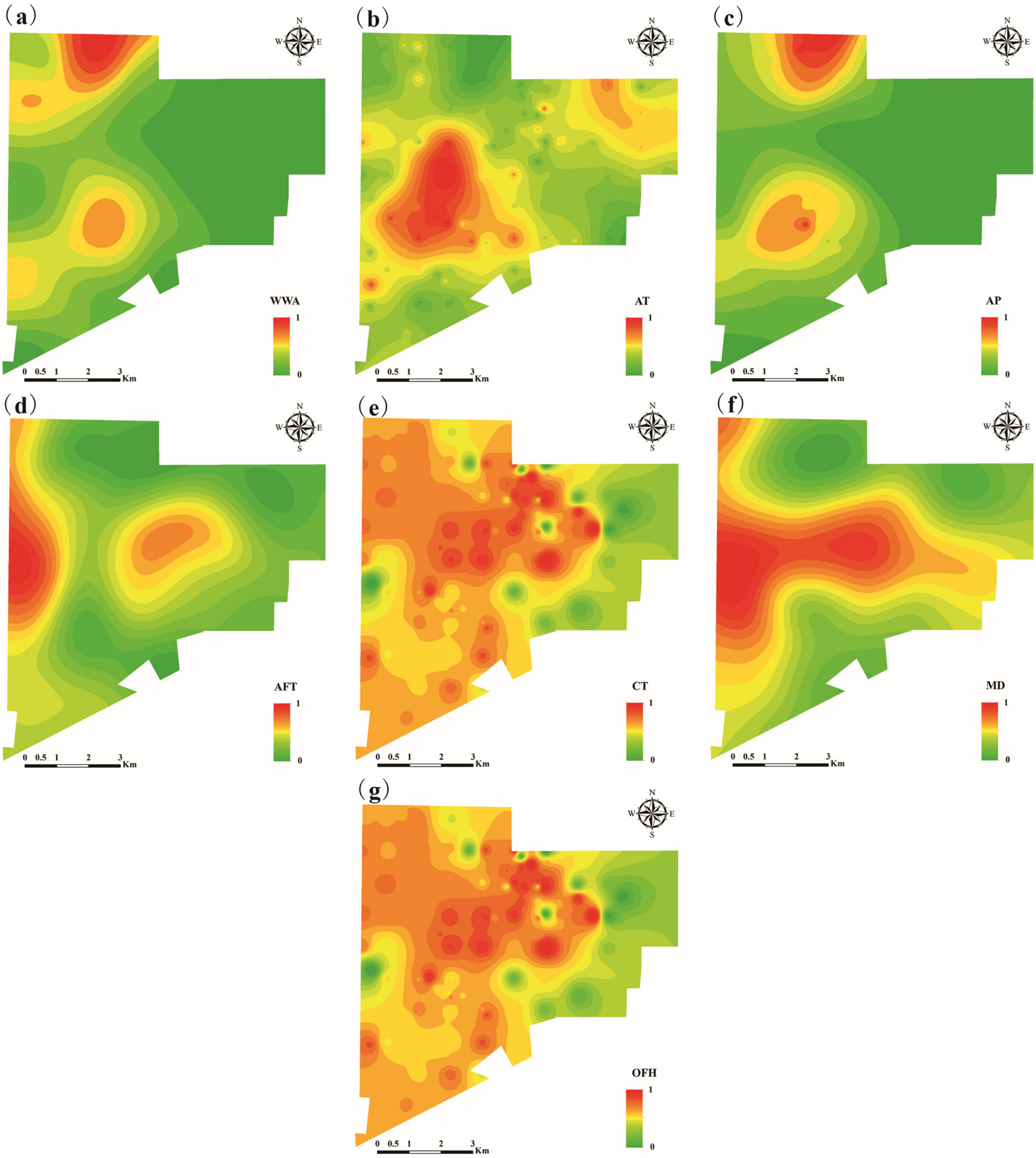

Figure 6. Thematic map of globally standardized evaluation factors: (**a**) WWA; (**b**) AT; (**c**) AP; (**d**) AFT; (**e**) CT; (**f**) MD; and (**g**) OFH.

4.1.2. Localized Standardization of Evaluation Indicators

The evaluation indicators were locally standardized using Equations (5) and (6), with a standardization circle radius of r = 500 m. Among these indicators, factors such as WWA, AP, AT, CT, MD, and OFH, which are positively correlated with roof water inrush risk, were standardized using Equation (5). On the other hand, the AFT, which is negatively correlated with roof water inrush risk, was standardized using Equation (6). The dimensionless maps of each evaluation criterion after local standardization were obtained using ArcGIS (Figure 7).

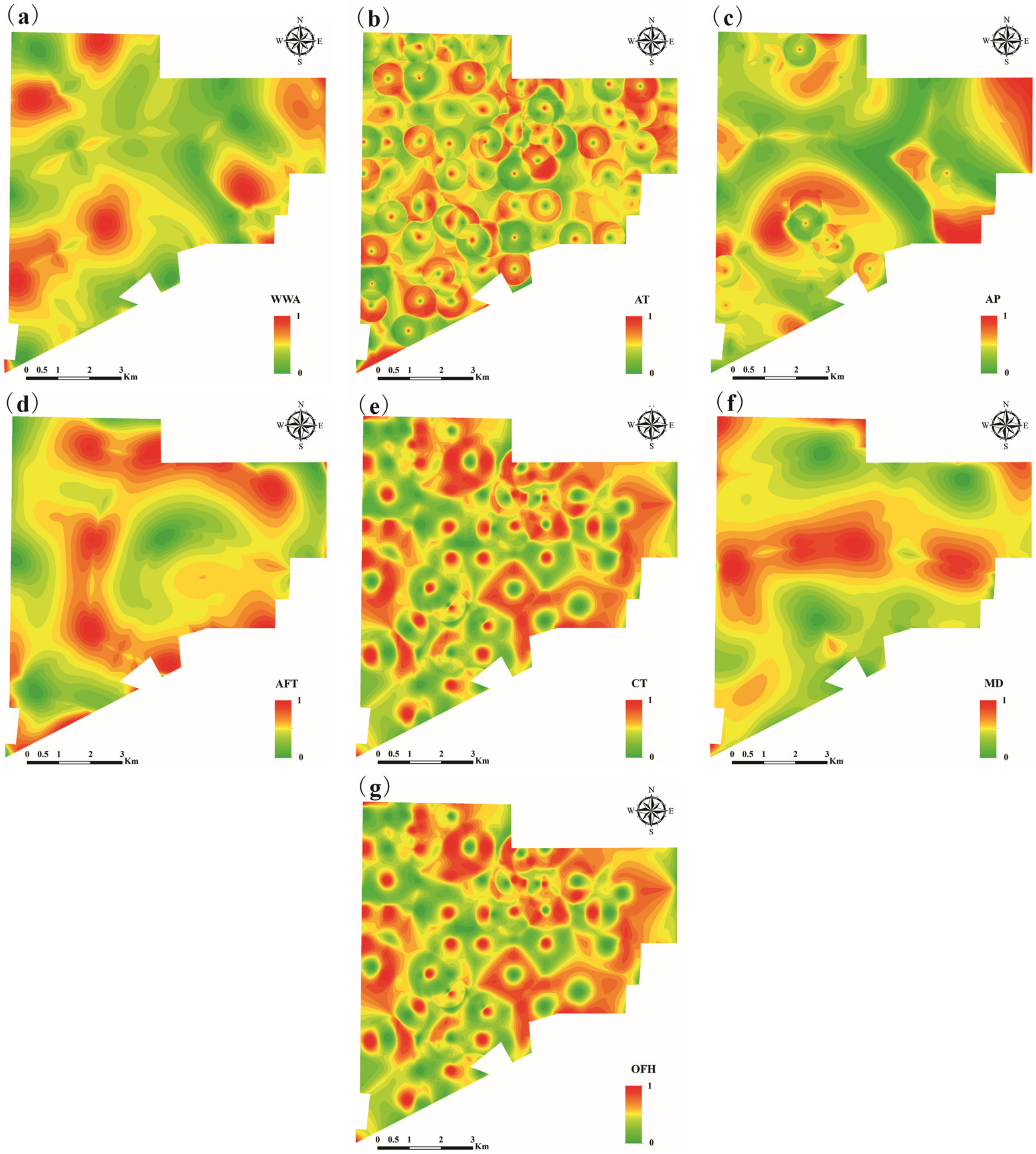

Figure 7. Dimensionless thematic maps of locally standardized evaluation factors: (**a**) WWA; (**b**) AT; (**c**) AP; (**d**) AFT; (**e**) CT; (**f**) MD; and (**g**) OFH.

4.2. Global Weights of Evaluation Indicators

Regarding the criteria weights, based on the probability distribution functions of the elements in the pairwise comparison judgment matrices, Monte Carlo simulation was employed to generate 10,000 judgment matrices using random sampling. After undergoing consistency testing with the AHP, 259 sets of qualified weight samples were obtained. Figure 8 depicts the probability density estimation of the criterion weight samples obtained through the MAHP method, while Figure 9 displays the distribution functions of the weights for the evaluation criterion [21].

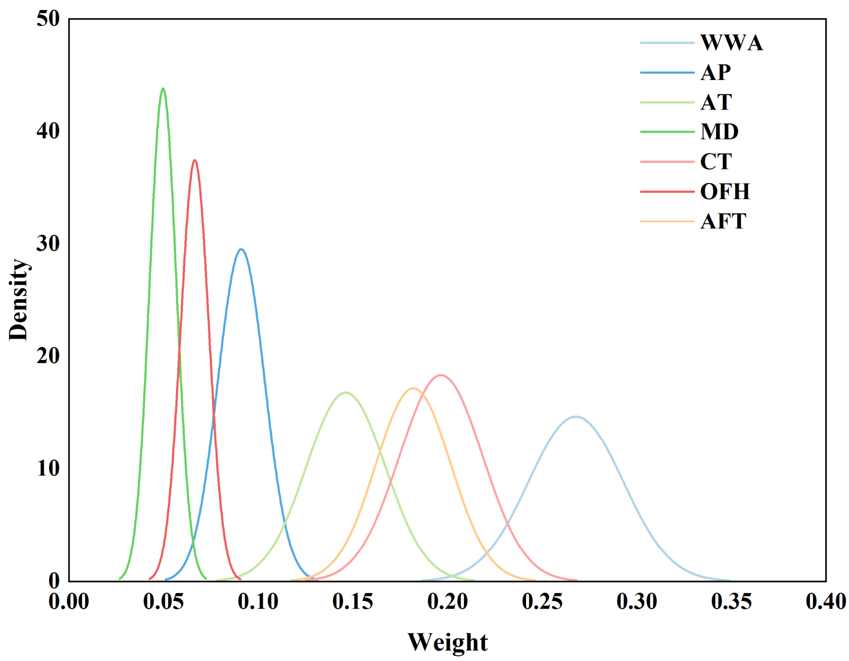

Figure 8. Curve depicting the distribution of weights for assessment indicators.

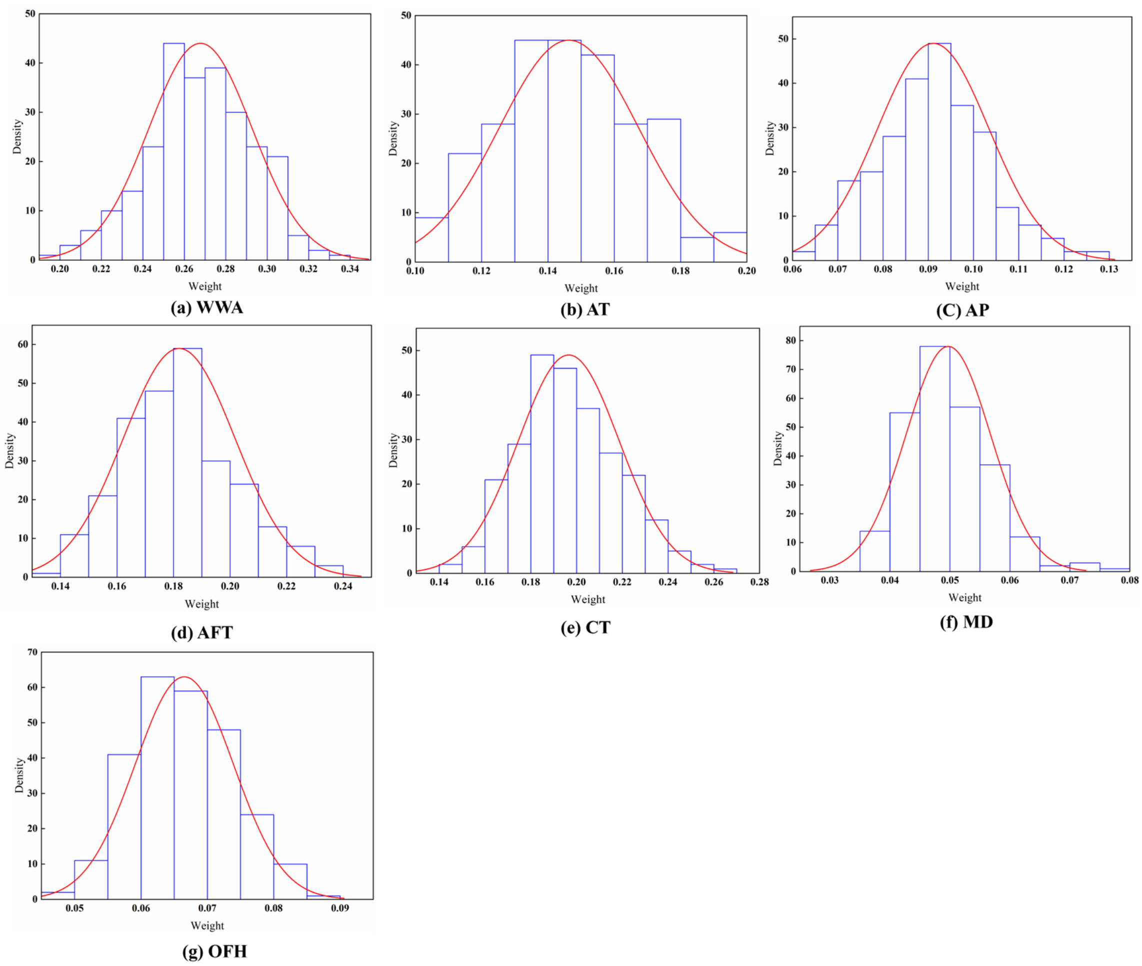

Figure 9. Evaluation indicators' weight distribution function [21].

Table 1 provides statistical data on criterion weights, with values in parentheses denoting the 95% confidence interval of the mean weights. An analysis of Table 1 and Figure 8 reveals that the majority of criterion weights, as determined by MAHP, are concentrated within a narrow confidence interval range around the mean. A narrower interval suggests greater concentration of weights and reduced uncertainty. This approach notably mitigates uncertainty in the process of determining indicator weights.

Table 1. Evaluation indicators' weight statistics.

Evaluation Indicators	Mean	Min	Max	Standardization	Confidence Interval
WWA	0.2678	0.1974	0.3301	0.02498	(0.2647–0.2708)
AP	0.0911	0.0633	0.1288	0.01233	(0.0895–0.0925)
AT	0.1463	0.1044	0.1985	0.0209	(0.1437–0.1488)
MD	0.0497	0.0370	0.0761	0.0070	(0.0488–0.0505)
CT	0.1965	0.1401	0.2613	0.0220	(0.1938–0.1992)
OFH	0.0665	0.0484	0.0875	0.0074	(0.0656–0.0674)
APT	0.1819	0.1395	0.2398	0.01979	(0.1795–0.1843)

In traditional AHP, the relative importance of evaluation indicators lacks clear differentiation due to differences among experts. Different experts may yield different rankings of criterion weights, leading to strong randomness and uncertainty. However, in this investigation, the MAHP method is employed, incorporating the probability density function of evaluation indicators to effectively address the randomness and uncertainty inherent in determining criterion weights. As a result, it yields a clear ranking of the weights of water inrush assessment indicators.

4.3. Evaluation Indicators' Local Weights

In ArcGIS, the local weight distribution maps of each evaluation indicator are calculated using Equation (7), as shown in Figure 10.

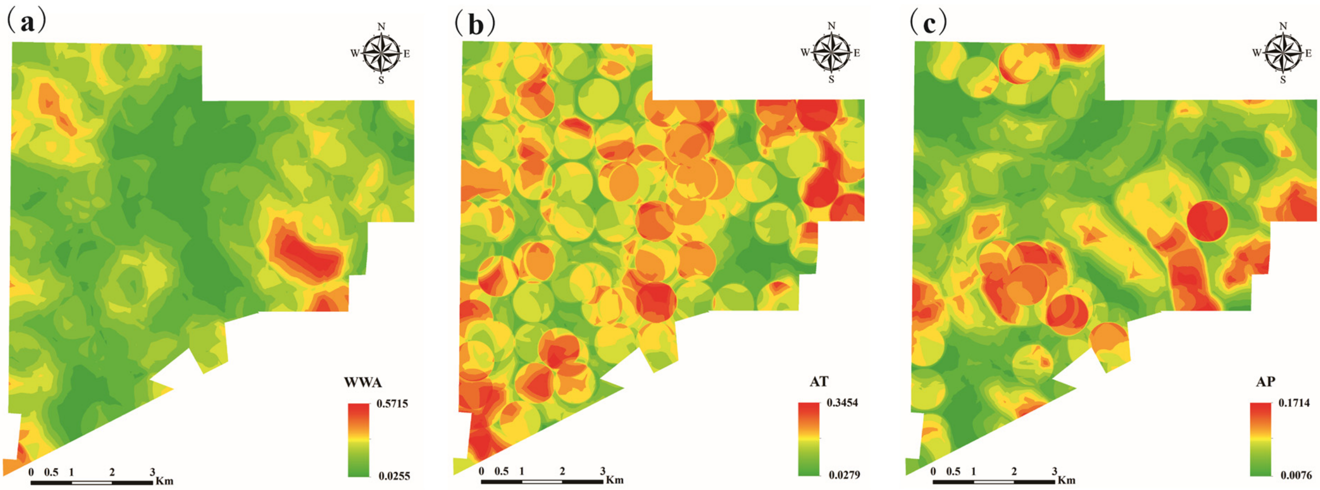

Figure 10. *Cont.*

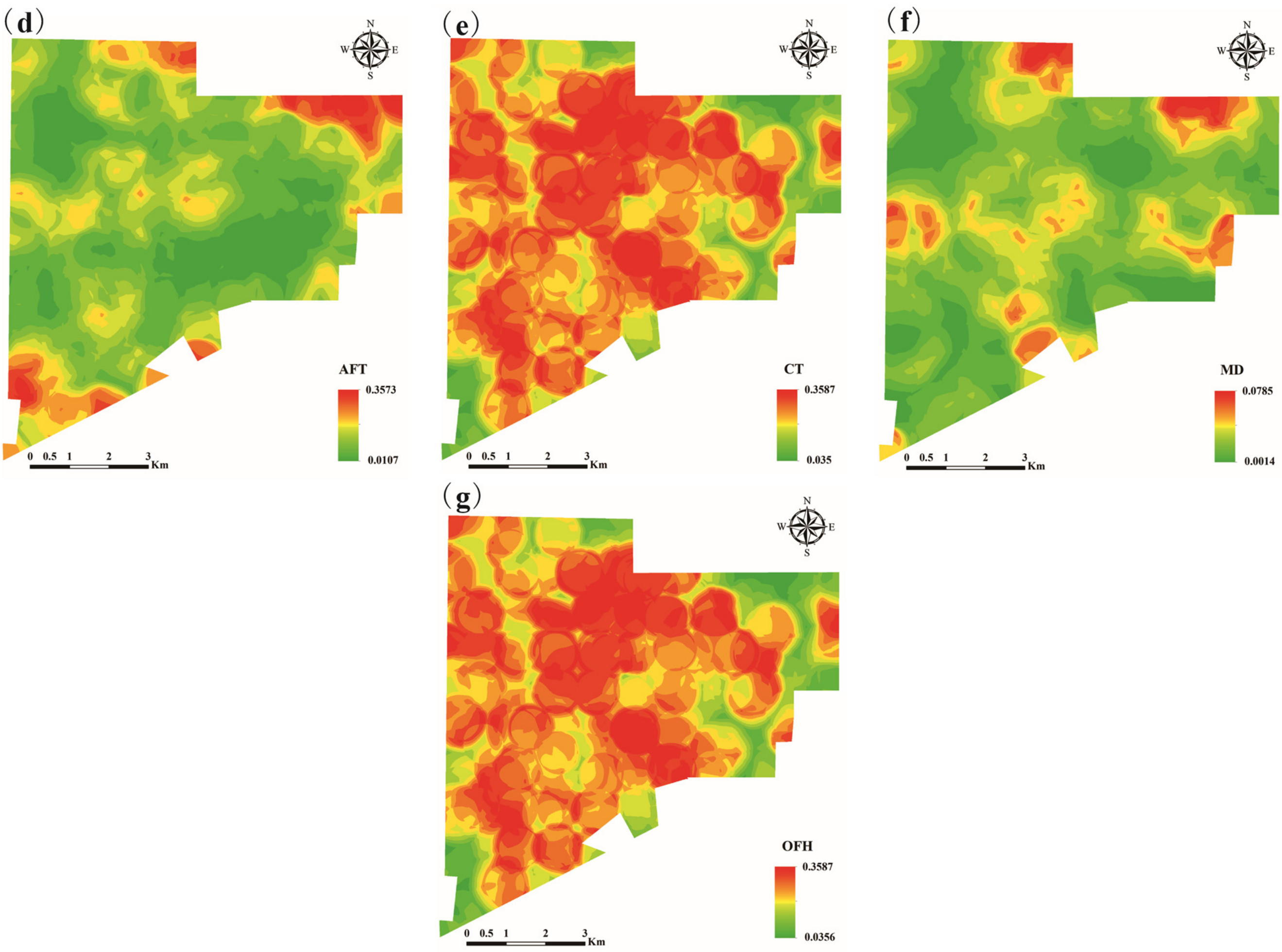

Figure 10. Local distribution of evaluation indicator weights: (**a**) WWA; (**b**) AT; (**c**) AP; (**d**) AFT; (**e**) CT; (**f**) MD; and (**g**) OFH.

4.4. Water Inrush Risk Evaluation Results

4.4.1. Global Evaluation Model

(1) Establishing the evaluation model.

Utilizing the weights of evaluation indicator s computed using MAHP, establish the global model for assessing the risk of roof water inrush, as shown in Equation (9):

$$\begin{aligned} RI(GA) = \ & 0.2678 f_1(x,y) + 0.0911 f_2(x,y) + 0.1463 f_3(x,y) + 0.0497 f_4(x,y) + \\ & 0.1965 f_5(x,y) + 0.0665 f_6(x,y) + 0.1819 f_7(x,y) \end{aligned} \tag{9}$$

where RI is the index of water inrush risk, and $f(x,y)$ is the dimensionless map of evaluation factors.

(2) Evaluation results of water inrush risk.

Using dimensionless maps of evaluation indicators obtained in Section 2 and the global evaluation mathematical model established in Section 4.4.1, the seven thematic maps of evaluation indicators are overlaid and integrated in ArcGIS to produce the water inrush risk zoning map under the global model evaluation, illustrated in Figure 11a. The risk zoning map is categorized into four risk zones, very high, high, low, and very low, employing the natural breaks method (Jenks) in GACGIS.

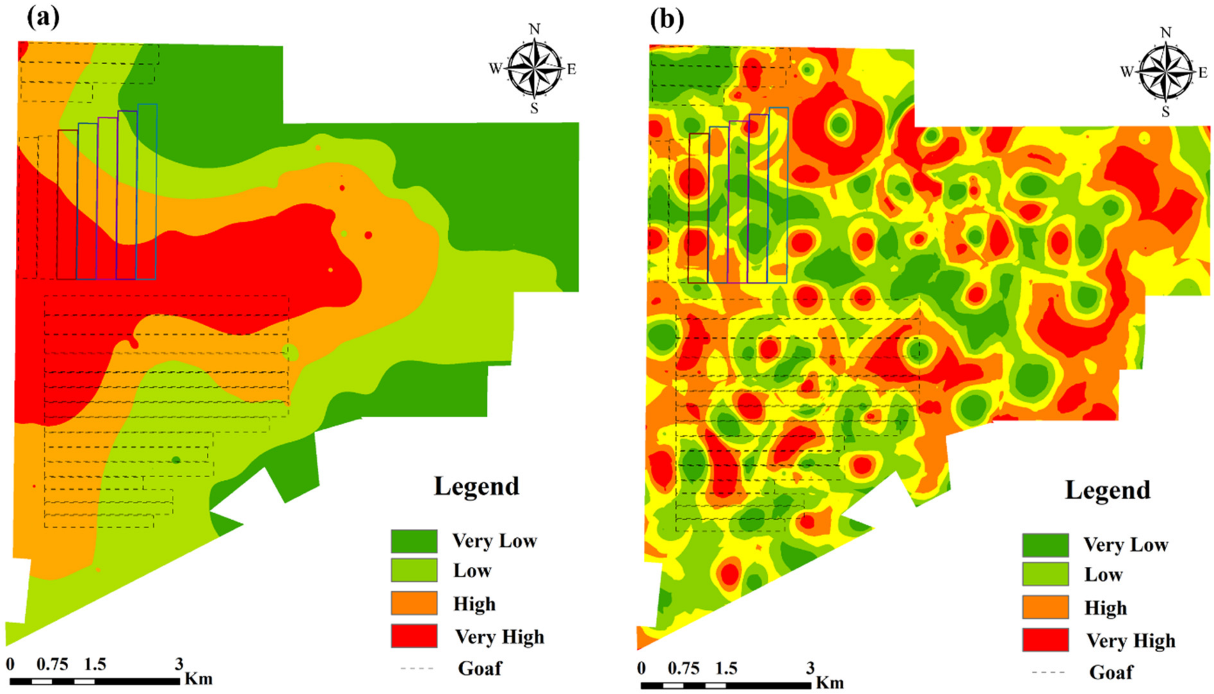

Figure 11. Water inrush risk evaluation results; (**a**) global model; (**b**) local model.

4.4.2. Local Evaluation Model

Based on the local water inrush risk assessment model established in Section 3.3, the non-dimensionalized maps of each evaluation indicator obtained in Section 4.1 were overlaid and integrated with their corresponding weight distribution maps in ArcGIS. This process resulted in the zoning map of roof water inrush risk, as shown in Figure 11b. Similarly, employing the Jenks in ArcGIS, the zoning map was categorized into four risk zones: very high, high, low, and very low.

4.5. Model Validation

This paper uses the geophysical anomaly area delineated by the Liangshuijing Coal Mine roof geophysical exploration method (the geophysical anomaly area is a high-risk area for roof water inrush) and the historical water inrush points to compare and verify the evaluation results of the two models and calculate the prediction accuracy (Table 2). The planar distribution of geophysical anomaly areas and historical water inrush points within the study area are depicted in Figure 12.

Table 2. Predictive accuracy of two models.

	Global Evaluation Model	Local Evaluation Model
Predictive accuracy of geophysical anomaly areas (%)	57.08	89.31
Predictive accuracy of water inrush points (%)	66.66	62.5
Average accuracy (%)	61.87	75.9

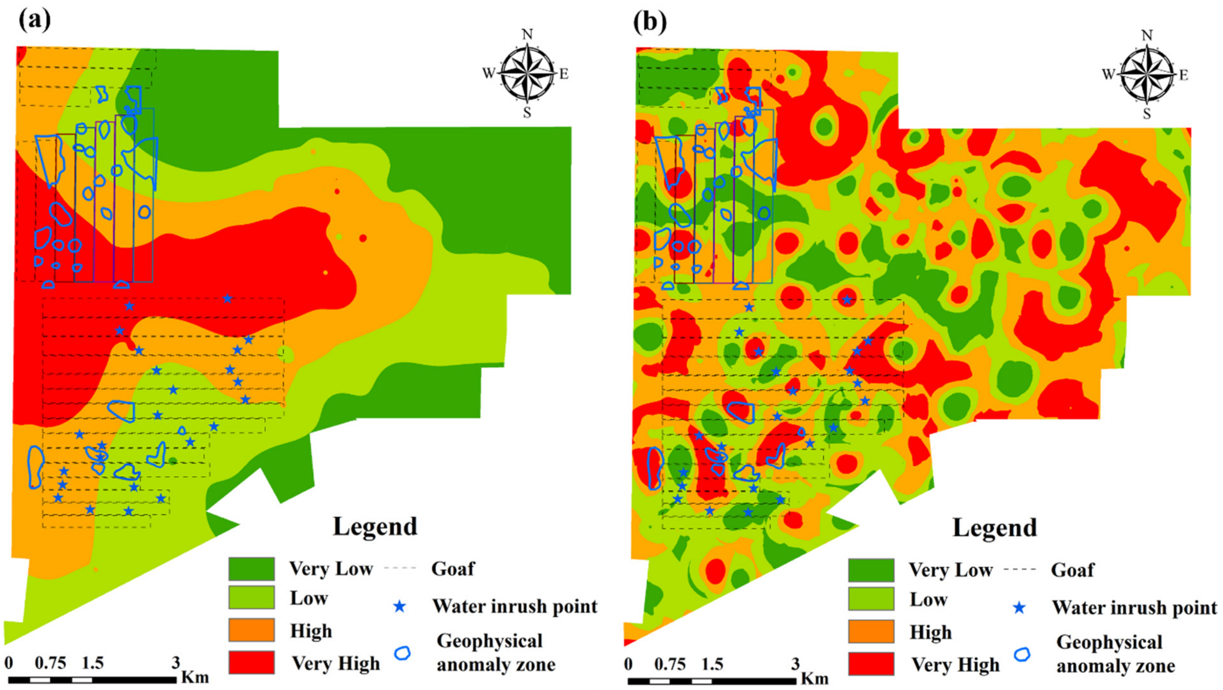

Figure 12. Evaluation result verification chart; (**a**) global evaluation model; (**b**) local evaluation model.

According to Table 2, there is a notable disparity in the predictive accuracy of the two models for the geophysical anomaly areas. The accuracy of the global evaluation model is 57.08%, whereas that of the local evaluation model is 89.31%. Therefore, the accuracy of the local evaluation model is higher than that of the global evaluation model. As for the predictive accuracy concerning historical water inrush points, the accuracy of the global evaluation model is 66.66%, while that of the local evaluation model is 62.5%. Thus, the accuracy of the global evaluation model is slightly higher than that of the local evaluation model.

From the perspective of the average accuracy of the two evaluation models, the local model is 75.9%, while the global model is 61.87%. This indicates that the predictive accuracy of the local evaluation model surpasses that of the global evaluation model. Therefore, the evaluation results of the local model are deemed to be more reliable and accurate compared to those of the global model.

5. Discussion

5.1. Comparison of the Spatial Distribution of Evaluation Indicator Attribute Values after Global and Local Standardization

A comparison of the global standardization results (Figure 6) and the local standardization results (Figure 5) reveals that: local standardization emphasizes spatial disparities, while global standardization emphasizes spatial similarities. The global standardization process can identify the overall spatial trends of the study area, while the local standardization process focuses more on the spatial trends of specific regions. Choosing the criterion of AT as a typical example for analysis can demonstrate the spatial pattern differences in attribute values between global and local standardization. Specifically, as shown in Figure 13, Figure 13a represents the global standardization results of the AT, while Figure 13b represents the local standardization results of AT. From Figure 13a, it can be observed that after global standardization, the larger values of the evaluation criteria tend to cluster in the northern and central parts of the study area, while the smaller standardized criterion values accumulate in the eastern and western parts of the study area. Conversely, Figure 13b illustrates that after local standardization, both the larger and smaller standardized criterion values of the evaluation indicators are relatively evenly distributed throughout the entire study area.

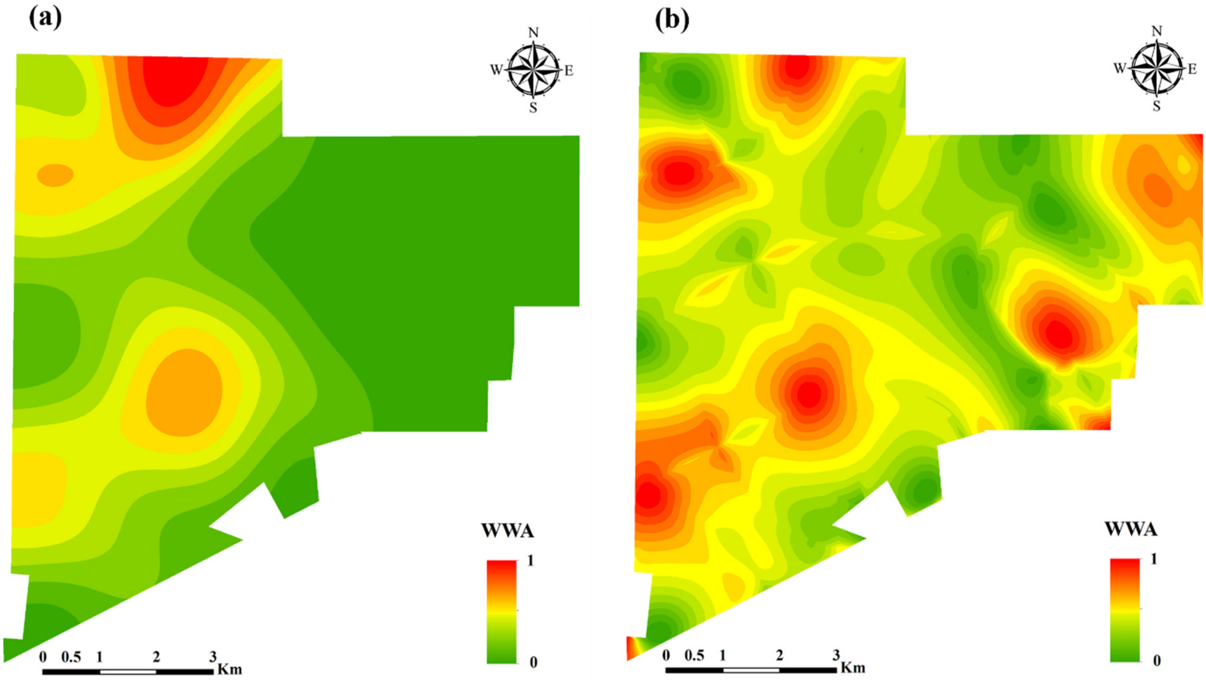

Figure 13. Distribution of AT attribute values; (**a**) global standardization; (**b**) local standardization.

5.2. Comparison of the Spatial Distribution of Global and Local Weights for Evaluation Indicators

Table 1 presents the global weight calculation results for the evaluation criteria, while Figure 10 illustrates the local weight calculation results for the same criteria. A comparison reveals that the global evaluation model assigns the evaluation criteria a constant value across the entire area, without considering variations in the importance of evaluation criteria due to spatial changes. Conversely, the local model can better address this issue, as it places greater emphasis on the importance of evaluation criteria at different locations. Using aquifer thickness as an example for analysis, the global evaluation model yields a fixed evaluation criterion weight of 0.2678, whereas the local weight calculation results fluctuate between 0.0279 and 0.3454 (Figure 10b). Due to the uneven distribution of aquifer thickness across the entire area, regions with greater thickness pose higher risks of water inrush. Therefore, in these areas, the evaluation indicator should be assigned a higher weight. Due to the uneven distribution of aquifer thickness across the entire area, regions with greater thickness pose higher risks of water inrush. Therefore, in these areas, the evaluation indicator should be assigned a higher weight. Conversely, in regions with thinner thickness, the risk of water inrush is lower, and, correspondingly, the weight assigned to this indicator should be smaller. If the evaluation indicator weight calculation results from the global model are used, this may lead to an overemphasis or underestimation of water inrush risk assessment results in the study area, which may not correspond to the actual situation. The weight calculation results of evaluation indicators from the local evaluation model can address this issue. This model adjusts the distribution of evaluation factor weights within the study area based on the relative magnitudes of evaluation criteria attribute values at different locations. Consequently, significant differences in weights across different locations are demonstrated, making the weight allocation results more reasonable.

5.3. Comparison of the Spatial Distribution of Water Inrush Risk Assessment Results between Global and Local Models

A comparison of the zoning maps depicting the water inrush risk assessment results from the two models (Figure 12) reveals distinct spatial patterns. The zoning map derived from the global evaluation model (Figure 12a) exhibits a relatively concentrated distribution of water inrush risk areas, with high-risk zones predominantly situated in the central part of the study area and low-risk zones primarily located in the peripheral regions. Conversely, the zoning map obtained from the local evaluation model (Figure 12b) demonstrates a more dispersed spatial distribution of high- and very high-risk areas. In regions where the global evaluation model initially identified concentrated areas of either high or low risk, the local evaluation model further differentiates risks within localized areas. To further compare the differences between the evaluation results obtained from the two models, the pixel counts within each risk level zone in the water inrush maps generated by the global and local models were separately compiled, as shown in Table 3.

Table 3. Pixel count statistics results for each risk zone.

	Global Evaluation Model	Local Evaluation Model
The number of pixels (count) within the very high- and high-risk zones.	906,962	781,558
The number of pixels (count) within the very low- and low-risk zones.	608,489	733,893

From Table 3, it can be observed that in the water rush risk assessment results obtained from the local evaluation model, there is a noticeable decrease in the proportion of very high and high-risk areas compared to the evaluation results from the global evaluation model. Simultaneously, there is an increase in the proportion of low- and very low-risk areas. This phenomenon is attributed to the adoption of local analysis methods, which accentuates the risk levels within localized regions, thereby reducing the generalization of risk levels caused by the global assessment of indicators. Furthermore, concerning the spatial distribution of high-risk areas, the water inrush risk zoning map obtained through local evaluation methods does not exhibit large-scale spatial clustering. Instead, high- and low-risk areas are distinguished across various regions within the study area.

In the evaluation results obtained from the global evaluation model, the high water inrush risk areas exhibit a large and concentrated area. This implies that coal mining enterprises will need to implement a significant number of flood prevention and control measures, as well as allocate considerable manpower and financial resources to manage these risk areas to ensure the safe operation of the mines. Undoubtedly, this leads to the wastage of resources, which is considered unreasonable [14,15,20,23].

The global evaluation model prioritizes increasing the accuracy of predictive results by sacrificing the area of safe zones, whereas the local evaluation model, while maintaining the same level of evaluation accuracy as or even exceeding that of the global evaluation model, reduces the area of high-risk zones. Furthermore, it delineates the distribution of water inrush zones in a more specific manner that aligns better with actual patterns. The reliability of water inrush risk assessment results obtained from the local evaluation model is notably higher than that of the global evaluation model. Moreover, the evaluation outcomes from the local evaluation model effectively pinpoint areas of high risk of roof water inrush, enhancing the targeting of water inrush prevention and control efforts. Therefore, local water inrush assessment emerges as a highly practical, rational, and necessary evaluation model for roof water inrush risk assessment work.

6. Conclusions

(1) This paper employed a Monte Carlo Analytic Hierarchy Process (AHP) method to calculate the global weights of evaluation criteria, establishing a global evaluation model for roof water inrush. Simultaneously, a circular window was utilized to traverse each position within the study area, standardizing the criterion indicators and calculating evaluation factor weights within the circular local range. This process facilitated the establishment of a local water inrush risk assessment model.
(2) Roof water inrush risk in the Liangshuijing mining area was evaluated using both global and local evaluation models, resulting in the generation of a zoning map for roof water inrush risk. Subsequently, the study area was divided into four categories of water inrush risk—very high, high, low, and very low—using the natural break method in GIS.
(3) Compared to the global evaluation model, the local evaluation model exhibits higher prediction accuracy. Moreover, it reduces the area of high-risk zones while achieving higher accuracy than the global evaluation model, resulting in a more specific delineation of the distribution of water inrush risk zones.
(4) The proposed local water inrush risk assessment model achieves higher accuracy and provides evaluation results that are more consistent with reality. It offers a more detailed delineation of water inrush risk areas, thereby providing a new evaluation method for water inrush risk assessment.

Author Contributions: Conceptualization, C.G., D.W. and J.M.; formal analysis, D.W. and C.G.; investigation, C.G., D.W., Y.F. and J.M.; methodology, C.G. and D.W.; project administration, K.L. and J.M. All authors have read and agreed to the published version of the manuscript.

Funding: The authors would like to acknowledge financial support from the National Natural Science Foundation of China under Grant grant (NO. 42172293) and the China Scholarship Council (CSC).

Data Availability Statement: This article contains no data or material other than the articles used for the review and referenced.

Acknowledgments: We would also like to acknowledge the reviewers for their invaluable comments.

Conflicts of Interest: Author Yafei Fang was employed by the company Shaanxi Energy Liangshuijing Mining Co., Ltd. The remaining authors declare that the research was conducted in the absence of any commercial or financial relationships that could be construed as a potential conflict of interest.

References

1. Li, P. Mine Water Problems and Solutions in China. *Mine Water Environ.* **2018**, *37*, 217–221. [CrossRef]
2. Zeng, Y.F.; Li, Z.; Gong, H.J.; Zheng, J. Water abundance characteristics in aquifer of weathered roof bedrock and prediction on water inrush risk. *Coal Eng.* **2018**, *50*, 100–104.
3. Dong, S.N.; Ji, Y.D.; Wang, H.; Zhao, B.F.; Cao, H.D.; Liu, Y.; Liu, Y.F.; Ji, Z.K.; Liu, B.G. Prevention and control technology and application of roof water disaster in Jurassic coal field of Ordos Basin. *J. China Coal Soc.* **2020**, *45*, 2367–2375.
4. The Coal Safety Network. Available online: https://www.mkaq.org/ (accessed on 30 March 2024).
5. Hu, W.Y.; Tian, G. Mine Water Disaster Type and Prevention and Control Counterm easures in China. *Coal Sci. Technol.* **2010**, *38*, 92–96.
6. Wu, Q.; Zhou, W.; Wang, J.; Xie, S. Prediction of groundwater inrush into coal mines from aquifers underlying the coal seams in China; application of vulnerability index method to Zhangcun coal mine, China. *Environ. Earth Sci.* **2009**, *57*, 1187–1195. [CrossRef]
7. Wu, Q.; Liu, Y.; Luo, L.; Liu, S.; Sun, W.; Zeng, Y. Quantitative evaluation and prediction of water inrush vulnerability from aquifers overlying coal seams in Donghuantuo coal mine, China. *Environ. Earth Sci.* **2015**, *74*, 1429–1437. [CrossRef]
8. Wu, Q.; Xu, K.; Zhang, W.; Wei, Z. Roof aquifer water abundance evaluation; a case study in Taigemiao, China. *Arab. J. Geosci.* **2017**, *10*, 254. [CrossRef]
9. Zeng, Y.; Wu, Q.; Liu, S.; Zhai, Y.; Lian, H.; Zhang, W. Evaluation of a coal seam roof water inrush: Case study in the Wangjialing coal mine, China. *Mine Water Environ.* **2018**, *37*, 174–184. [CrossRef]
10. Wu, Q.; Liu, Y.; Zhou, W.; Li, B.; Zhao, B.; Liu, S.; Sun, W.; Zeng, Y. Evaluation of water inrush vulnerability from aquifers overlying coal seams in the Menkeqing coal mine, China. *Mine Water Environ.* **2015**, *34*, 258–269. [CrossRef]

11. Wu, Q.; Guo, X.; Shen, J.; Xu, S.; Liu, S.; Zeng, Y. Risk Assessment of Water Inrush from Aquifers Underlying the Gushuyuan Coal Mine, China. *Mine Water Environ.* **2017**, *36*, 96–103. [CrossRef]
12. Wu, Q.; Zhang, Y.; Liu, Y. Using the Vulnerable Index Method to Assess the Likelihood of a Water Inrush through the Floor of a Multi-seam Coal Mine in China. *Mine Water Environ. J.* **2011**, *25*, 54–60. [CrossRef]
13. Wu, Q.; Zhao, D.; Wang, Y.; Shen, J.; Mu, W.; Liu, H. Method for assessing coal-floor water-inrush risk based on the variable-weight model and unascertained measure theory. *Hydrogeol. J.* **2017**, *25*, 2089–2103. [CrossRef]
14. Li, Q.; Sui, W. Risk evaluation of mine-water inrush based on principal component logistic regression analysis and an improved analytic hierarchy process. *Hydrogeol. J.* **2021**, *29*, 1299–1311. [CrossRef]
15. Cheng, X.; Qiao, W.; Li, G.; Yu, Z. Risk assessment of roof water disaster due to multi-seam mining at Wulunshan Coal Mine in China. *Arab. J. Geosci.* **2021**, *14*, 1116. [CrossRef]
16. Liu, M.; Qiao, W.; Meng, Q.; Bu, Z. A new risk zoning method for water inrush from separated layers at coal mines: A case study, Cuimu coal mine, China. *Arab. J. Geosci.* **2021**, *14*, 2544. [CrossRef]
17. Wang, D.; Sui, W.; Ji, Z. Fault complexity degree in a coal mine and the implications for risk assessment of floor water inrush. *Geomat. Nat. Hazards Risk* **2024**, *15*, 2293464. [CrossRef]
18. Gao, C.; Wang, D.; Liu, K.; Deng, G.; Li, J.; Jie, B. A Multifactor Quantitative Assessment Model for Safe Mining after Roof Drainage in the Liangshuijing Coal Mine. *ACS Omega* **2022**, *7*, 26437–26454. [CrossRef]
19. Zhao, Z.; Gu, J. Risk Evaluation of Mine-Water Inrush Based on Comprehensive Weight Method. *Geotech. Geol. Eng.* **2023**, *41*, 189–203. [CrossRef]
20. Li, L.; Li, W.; Zhou, S.; He, J.; Chen, W.; Wang, Q. An improved risk zoning method of bed-separation water inrush in underground coal mines: A case study in Ningxia, China. *Environ. Sci. Pollut. Res. Int.* **2023**, *30*, 57518–57528. [CrossRef]
21. Zhao, B.; Liu, Q.; Zhu, J. Risk Assessment and Zonation of Roof Water Inrush Based on the Analytic Hierarchy Process, Principle Component Analysis, and Improved Game Theory Method. *Sustainability* **2023**, *15*, 11375. [CrossRef]
22. Wang, D.; Gao, C.; Liu, K.; Gong, J.; Fang, Y.; Xiong, S. A GIS-Based Probabilistic Spatial Multicriteria Roof Water Inrush Risk Evaluation Method Considering Decision Makers' Risk-Coping Attitude. *Water* **2023**, *15*, 254. [CrossRef]
23. Liu, Q.; Xu, J.; Wang, Q.; Li, W. Risk Assessment of Water Inrush from Coal Seam Roof Based on the Combined Weighting of the Geographic Information System and Game Theory: A Case Study of Dananhu Coal Mine No. 7, China. *Water* **2024**, *16*, 710. [CrossRef]
24. Rosenbloom, E.S. A probabilistic interpretation of the final rankings in AHP. *Eur. J. Oper. Res.* **1997**, *96*, 371–378. [CrossRef]
25. Hsu, T.; Pan, F.F.C. Application of Monte Carlo AHP in ranking dental quality attributes. *Expert. Syst. Appl.* **2009**, *36*, 2310–2316. [CrossRef]
26. Wang, C.; Yang, S.; Jiang, C.Y.; Wu, G.Y.; Liu, Q.Z. Monte Carlo analytic hierarchy process for selection of the longwall mining method in thin coal seams. *J. S. Afr. Inst. Min. Metall.* **2019**, *119*, 1005–1012.
27. Ataei, M.; Shahsavany, H.; Mikaeil, R. Monte Carlo Analytic Hierarchy Process (MAHP) approach to selection of optimum mining method. *Int. J. Min. Sci. Technol.* **2013**, *23*, 573–578. [CrossRef]
28. Tang, Z.; Yi, S.; Wang, C.; Xiao, Y. Incorporating probabilistic approach into local multi-criteria decision analysis for flood susceptibility assessment. *Stoch. Env. Res. Risk A* **2018**, *32*, 701–714. [CrossRef]
29. Tang, Z.; Zhang, H.; Yi, S.; Xiao, Y. Assessment of flood susceptible areas using spatially explicit, probabilistic multi-criteria decision analysis. *J. Hydrol.* **2018**, *558*, 144–158. [CrossRef]
30. Xiao, Y.; Yi, S.; Tang, Z. A Spatially Explicit Multi-Criteria Analysis Method on Solving Spatial Heterogeneity Problems for Flood Hazard Assessment. *Water Resour. Manag.* **2018**, *32*, 3317–3335. [CrossRef]
31. Malczewski, J.; Liu, X. Local ordered weighted averaging in GIS-based multicriteria analysis. *Ann. GIS* **2014**, *20*, 117–129. [CrossRef]